Study of phosphate removal from aqueous solution by zinc oxide

Zhen Luo, Suiyi Zhu, Zhongmou Liu, Jiancong Liu, Mingxin Huo and Wu Yang

ABSTRACT

Zinc oxide (ZnO) was synthesized and used to investigate the mechanism of phosphate removal from aqueous solution. ZnO particles were characterized by X-ray diffraction, scanning electron microscope and Fourier transform infrared spectroscopy before and after adsorption. Batch experiments were carried out to investigate the kinetics, isotherms, effects of initial pH and co-existing anions. The adsorption process was rapid and equilibrium was almost reached within 150 min. The adsorption kinetics were described well by a pseudo-second-order equation, and the maximum phosphate adsorption capacity was 163.4 mg/g at 298 K and pH $\sim 6.2 \pm 0.1$. Thermodynamic analysis indicated the phosphate adsorption onto ZnO was endothermic and spontaneous. The point of zero charge of ZnO was around 8.4 according to the pH-drift method. Phosphate adsorption capacity reduced with the increasing initial solution pH values. The ligand exchange and Lewis acid-base interaction dominated the adsorption process in the lower and the higher pH range, respectively. Nitrate, sulfate and chloride ions had a negligible effect on phosphate removal, while carbonate displayed significant inhibition behavior.

Key words | adsorption, kinetics, phosphate, thermodynamics, zinc oxide

Zhen Luo
Suiyi Zhu
Zhongmou Liu
Jiancong Liu
Mingxin Huo
Wu Yang (corresponding author)
School of Environment,
Northeast Normal University,
Changchun 130117,
China
E-mail: yangw104@gmail.com

INTRODUCTION

As a principal nutrient, phosphate (P) plays a vital role in ecosystems. However, if excessive amounts of phosphate, released from agricultural fertilizer runoff, municipal wastewater, or effluent from chemical and food processing industries, are discharged into water bodies, there might be overgrowth of aquatic plants, depletion of dissolved oxygen and subsequent deterioration of water quality. Accordingly, it is necessary to reduce the phosphate concentration and control the discharge of phosphate.

To achieve this goal, various techniques, including chemical precipitation, biological removal, adsorption, crystallization and anion exchange, have been studied (Morse *et al.* 1998). However, the biological process is not steady and relies heavily on water quality, and chemical precipitation can be subject to problems with sludge treatment and disposal (Yeon *et al.* 2008). Anion exchange also has drawbacks, e.g., low selectivity in the presence of competing

anions (Tsuji 2002). Compared with the traditional methods mentioned above, adsorption provides faster phosphate removal (Chouyyok *et al.* 2010), and can be applied to different phosphate concentrations under various environmental conditions (Wang *et al.* 2007; Haghseresht *et al.* 2009; Rentz *et al.* 2009; Pitakteeratham *et al.* 2013). It is considered a promising technique for removing phosphate. For this reason, a great many low-cost and easily available materials, including industrial by-products, natural materials, metal-modified minerals, man-made products, inorganic–organic hybrid materials and metal oxide/multi-metal composite oxides have been tested (Liao *et al.* 2006; Mohan & Pittman 2007; Vohla *et al.* 2011; Jiang & Ashekuzzaman 2012).

Zinc oxide (ZnO), as an environment-friendly material (Wan 2006), has been used for diverse applications (Hariharan 2006; Wang *et al.* 2011; Moezzi *et al.* 2012) and is considered a mature engineering material with annual

production of one and a half million tons (Moezzi *et al.* 2012). Kikuchi *et al.* (2006) have reported its sorption performance toward metal ions and Liufu *et al.* (2004) investigated the effect of polyethylene glycol on the adsorption onto ZnO/ polymer solution interface, and found that the blockage of the adsorption sites played a major role in the change of zeta potential. Regarding phosphorus, Namasivayam & Sangeetha (2004) found that ZnCl$_2$-activated carbon developed from coir pith is a good sorbent for phosphate adsorption over a wide pH range (pH ∼ 3–10). Moreover, Cheng *et al.* (2009) and Zhou *et al.* (2011) reported that zinc-aluminum hydroxides (oxides) can effectively remove phosphate with a high content of ZNO at a Zn/Al molar ratio of 2, sintered at 573 K. He *et al.* (2010) reported that ZnAl layered double hydroxides show selective adsorption of phosphate and the calcined samples possibly proceed through ligand complexation or electrostatic attraction between phosphate ions and hydrated ZnO formed after calcination. However, up to now, phosphate adsorption by more stable ZnO particles has not been reported.

In the present study, ZnO was synthesized and used to investigate the mechanism of phosphate removal. The effect of pH and co-existing anions on phosphate capture, as well as the adsorption isotherm and kinetics, were evaluated. X-ray diffraction (XRD), scanning electron microscope (SEM) and Fourier transform infrared spectroscopy (FT-IR) were also performed to preliminarily elucidate the underlying sorption mechanism of ZnO. With this information, a better understanding of adsorption behaviors and properties could be obtained, and the feasibility of the use of ZnO in water/waste water will become clearer.

MATERIALS AND METHODS

Materials

All chemicals of analytical grade were purchased from the Tianjin Fuchen Chemical Reagents Factory (Tianjin, China), and used without any further purifications. ZnO particles were fabricated by the chemical precipitation-thermal decomposition method with minor modifications. In brief, 0.1 M NaOH solution was dropwise added into 80 mL distilled water containing 10 g of ZnSO$_4$·7H$_2$O with continuous

stirring, until the solution pH reached around 8 ± 0.1. The suspended solution was stirred for 3 h at room temperature. The obtained pastes were harvested by repeating the following procedure three times: centrifuging the solution at 4,000 rpm for 5 min, and then washing with distilled water. The pastes were then put into the Muffle furnace and kept at 573 K for 6 h (Zhou *et al.* 2011) to produce the ZnO particles. The obtained ZnO particles were ground into powder with an agate mortar and kept in a dryer for further use.

Analytical methods

All the samples were filtered through 0.45 μm membranes before determination. Phosphate concentrations were determined by a Metrohm 881 ion chromatograph coupled with a Metrosep A Supp 4 column. A solution comprising 1.8 mM of Na$_2$CO$_3$ and 1.7 mM of NaHCO$_3$ was used as a mobile phase at a flow rate of 1.2 mL/min.

Phosphate adsorption capacities (q_e, mg P/g) were determined by the following equation:

$$q_e = \frac{V \times (C_o - C_e)}{1{,}000 \times m} \tag{1}$$

$$\text{removal efficiency}\,(\%) = \left(1 - \frac{C_e}{C_o}\right) \times 100\% \tag{2}$$

where V (mL) was the volume of the working solution, C_o and C_e (mg/L) were the concentration in the working solution and filtrate, respectively, and m (g) was the adsorbent mass.

The surface morphology and element composition of the ZnO particles were obtained by a SUTW-Sapphire system with energy dispersive X-ray analysis (EDAX) (PHILIPS XL30 ESEM, Eindhoven, The Netherlands). The XRD pattern was used to characterize the relative intensity of ZnO particles, which were fabricated as described in the 'Materials' section above, and recorded by a Bruker D8 Advance (Bruker, Bremen, Germany) using Cu Kα radiation within the 2θ range of 4–90°. The FT-IR spectroscopy was obtained using a Vertex 70 with a DTGS (deuterated triglycine sulfate) detector (Bruker, Bremen, Germany) at 4,000–400 cm^{-1}, with a pellet of powdered potassium bromide. For comparison, the XRD, SEM and FT-IR of the ZnO particles after adsorption were also conducted.

Experimental procedures

A series of batch experiments was conducted to investigate the characteristics of phosphate adsorption onto ZnO. Kinetic experiments were performed by sampling a 2 mL solution from the 1,000 mL working solution containing 400 ± 0.03 mg of ZnO particles and the desired concentration of working solution (10, 20 and 30 mg/L) at various shaking times (0, 5, 10, 20, 30, 45, 60, 90, 150, 270, 390 510, 690 min) in an incubator shaker (WR-1, Shanghai, China) at 298 K.

Sorption isotherm experiments were conducted in 50 mL sealed Erlenmeyer flasks containing 25 mL working solution and 10 ± 0.03 mg of ZnO particles with various phosphate concentrations (0–100 mg/L) and a shaking time of 690 min at desired temperatures.

To determine the effect of pH, 10 ± 0.03 mg of ZnO particles was added into 50 mL Erlenmeyer flasks containing 25 mL working solution (20 mg/L) at desired pH values (3–11) adjusted by 0.1 M HCl and 0.1 M NaOH solution at 298 K. These flasks were sealed with parafilms (Pechiney Plastic Packaging Co., Washington, NJ, USA), and then transferred into the incubator shaker for 1,440 min. The solutions were then filtered through 0.45 μm membranes to determine the equilibrium pH. The concentrations of the releasing Zn^{2+} were determined by inductively coupled plasma (ICP) (PLASMA-SPEC I, Shelton, CT, USA).

The effects of co-existing anions (sulfate, carbonate, nitrate and chloride ion) on phosphate adsorption were investigated in 25 mL working solution (20 mg/L and 10 ± 0.03 mg of ZnO particles), which contained 10 or 20 mg/L of SO_4^{2-}, CO_3^{2-}, NO_3^-, or Cl^- ions at 298 K.

All working solutions were directly diluted from phosphate stock solution (counted as P, 1,000 mg/L) and each of the experiments was conducted twice.

RESULTS AND DISCUSSION

SEM and XRD

According to the SEM photographs shown in Figure 1, ZnO particles exhibited individual, sheet morphologies and the particles formed aggregates of different sizes. The EDAX
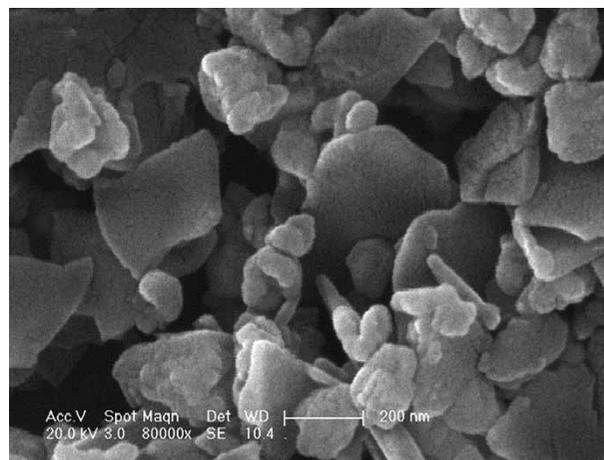

Figure 1 | SEM photograph of ZnO particles after phosphate adsorption.

spectrum of ZnO particles after phosphate adsorption was also analyzed and the P element occurred in the EDAX spectrum (Figure S1, in the supporting information, available online at http://www.iwaponline.com/jwh/013/210.pdf), which confirmed the presence of phosphate on the surface of the ZnO particles after adsorption.

Figure 2 shows the XRD results of fresh ZnO samples and ZnO samples obtained from the kinetic experiments. The strong and narrow peaks indicate that the adsorbent was well crystallized during the calcination process. The diffraction peaks of ZnO samples before and after adsorption correspond well with the standard data for ZnO (Zincite, syn. JCPDS card #36-1451).
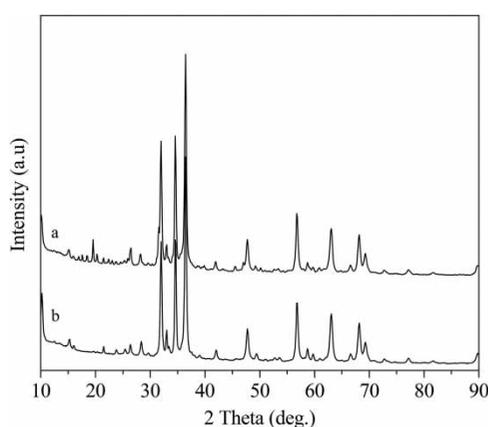

Figure 2 | XRD patterns of ZnO (a) ZnO after adsorption (b) ZnO before phosphate adsorption.

FT-IR analysis

The FT-IR spectra of fresh and phosphate-loaded ZnO particles are presented in Figure S2 (available online at http://www.iwaponline.com/jwh/013/210.pdf). The broad peaks apparent around the 3,400–1,630 cm^{-1} region might be attributed to the existence of the O-H stretching and bending vibrations, which were mainly caused by the adsorbed H$_2$O molecules (Lv *et al.* 2013; Zhang *et al.* 2013). The peaks appearing at around 1,114, 1,069 and 965 cm^{-1} might be assigned to the vibration of SO$_4^{2-}$ (Wang *et al.* 2006) from the raw materials (ZnSO$_4$·7H$_2$O). The peaks presenting at around 415–425 cm^{-1} might correspond to the stretching frequency of Zn-O (Musić *et al.* 2002; Prasad *et al.* 2006). After adsorption, marked peaks appearing at 1,026, 1,006 and 945 cm^{-1} might be attributable to the symmetrical stretching vibration of phosphate (Arai & Sparks 2001; Ning *et al.* 2013). The peak at 965 cm^{-1} disappearing after phosphate adsorption might be covered by that of phosphate. It is also noteworthy that the frequency of Zn-O vibration moved from 415 to 425 cm^{-1} after uptake of phosphate, which might be due to the fact that the active sites reacted with phosphate.
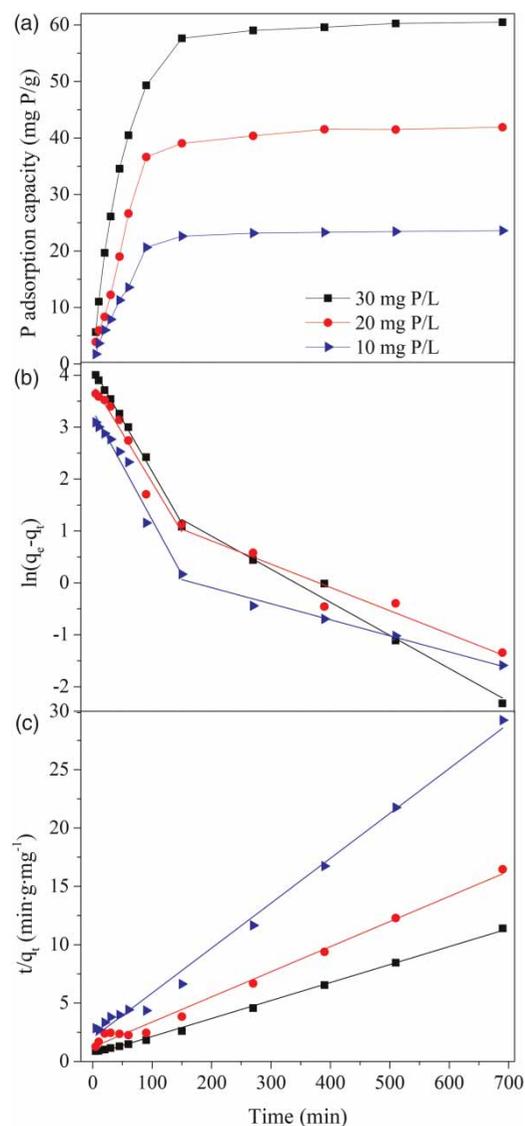
Kinetics

The experimental data obtained as a function of reaction time were analyzed using the pseudo-first-order (Equation (3)) and pseudo-second-order (Equation (4)) kinetic models:

$$\ln(q_e - q_t) = \ln q_e - k_1 t \qquad (3)$$

$$t/q_t = 1/k_2 q_e^2 + t/q_e \qquad (4)$$

where q_e and q_t (mg P/g) were the amounts of phosphate adsorbed on ZnO at equilibrium and time t (min), respectively, k_1 (min^{-1}) was the rate constant of the pseudo-first-order kinetic model and k_2 (g/(mg·min)) was the rate constant of the pseudo-second-order kinetic model.

As can be seen from Figure 3(a), the phosphate adsorption capacity of ZnO increased rapidly in the first 150 min, and then gradually increased until the equilibrium was reached at 510 min. The further extension of contact time did not affect the adsorption amounts of ZnO noticeably.

Figure 3 | Kinetic behaviors of phosphate adsorption onto ZnO. (a) Effect of contact time and initial phosphate concentration. (b) Pseudo-first-order kinetic model for phosphate adsorption. (c) Pseudo-second-order kinetic model for phosphate adsorption.

The phosphate adsorption amount increased with the increasing initial phosphate concentration (from 23.6 mg P/g in 10 mg/L to 60.5 mg P/g in 30 mg/L).

To further study the phosphate adsorption onto ZnO, the adsorption kinetic data were fitted to an integrated first (or second)-order kinetic expression, and are presented in Figure 3(b) and 3(c); the fitting parameters are listed in Table 1. According to the first-order kinetic model, the adsorption process could be divided into two parts by the

Table 1 │ Comparison of the pseudo-first- and second-order adsorption rate constants and experimental values for different initial phosphate concentrations

C_o (mg P/L)	$q_{e\,(exp)}$ (mg P/g)	Pseudo-second-order kinetics			Pseudo-first-order kinetics					
		k_2 (g/(mg·min))	$q_{e\,(cal)}$ (mg P/g)	R^2	k_{p1} (min^{-1})	$q_{e1\,(cal)}$ (mg P/g)	R^2	k_{p2} (min^{-1})	$q_{e2\,(cal)}$ (mg P/g)	R^2
10	23.6	7.3×10^{-4}	26.0	0.994	2.0×10^{-2}	27.6	0.997	6.4×10^{-3}	1.7	0.978
20	41.9	3.4×10^{-4}	46.5	0.991	1.9×10^{-2}	46.3	0.952	4.5×10^{-3}	5.5	0.920
30	60.5	4.0×10^{-4}	64.9	0.998	2.1×10^{-2}	62.5	0.969	3.1×10^{-3}	8.8	0.977

adsorption rate constant ($k_{p1} > k_{p2}$, k_{p1} and k_{p2} were the rate constant of fast and slow adsorption phase, respectively, and the values are listed in Table 1), i.e., fast adsorption and slow adsorption, which were also verified by the effect of contact time on the adsorption process shown in Figure 3(a). The fast adsorption process might be attributed to electrostatic attraction, or the driving force of a concentration gradient at higher initial phosphate concentration, which resulted in the rapid transportation of phosphate to the surface of the adsorbent, with respect to that of the adsorbent surface. The following slow adsorption process suggests that the driving force of the concentration gradient became weaker or the intraparticle diffusion dominated the adsorption process at that stage.

In addition, the pseudo-second-order model was also introduced to fit the kinetic data, and the results suggest that the adsorption of phosphate onto ZnO was chemisorption, or chemical bonding between adsorbent-active sites (Wang *et al.* 2006). That conclusion could also be supported by the close values of $q_{e(exp)}$ and $q_{e(cal)}$ of the pseudo-second-order model.

Isotherms

The experimental data obtained as a function of initial phosphate concentrations were analyzed using Langmuir (Equations (5) and (6)) and Freundlich (Equation (7)) models:

$$q_e = bq_mC_e/(1 + bC_e) \tag{5}$$

$$R_L = \frac{1}{1 + b \times C_o} \tag{6}$$

$$\ln q_e = \ln K_f + \frac{1}{n}\ln C_e \tag{7}$$

where, q_m (mg P/g) was the theoretical maximum phosphate adsorption capacity, C_o and C_e (mg/L) were phosphate concentrations in working solution and equilibrium solution, respectively, b (L/mg) was the affinity constant, R_L was a dimensionless affinity constant, known as a separation factor adsorption, which indicated the adsorption nature to be either unfavorable ($R_L > 1$), linear ($R_L = 1$), favorable ($0 < R_L < 1$) or irreversible ($R_L = 0$), and K_f (mg/g) and n were Freundlich constants.

The adsorption of phosphate onto ZnO at different temperatures was fitted by Langmuir and Freundlich isotherm models and is depicted in Figure 4. According to Table 2, at 298 K, the isotherm data could be better fitted by the Langmuir model rather than the Freundlich model, indicating that the production of zinc phosphate might be neglected because the Langmuir model could have the optimum performance to characterize the adsorption processes without precipitation (Del Bubba *et al.* 2003). Comparing the values of parameter R_L (Figure S3, available online at http://www.iwaponline.com/jwh/013/210.pdf), it is suggested that the adsorption of phosphate was more favorable at higher initial concentrations than at lower ones (Foo & Hameed 2010).
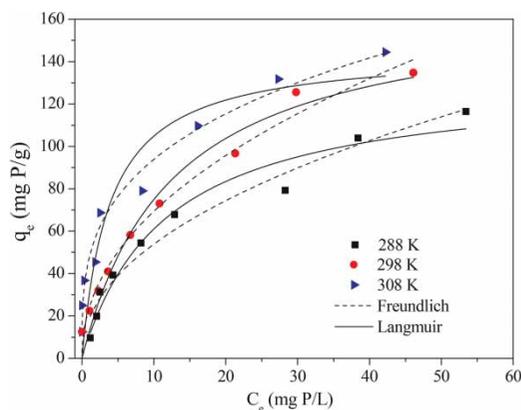
Figure 4 │ Langmuir and Freundlich isotherms of ZnO at 288, 298, and 308 K.

Table 2 │ Langmuir and Freundlich isotherm parameters for phosphate adsorption onto ZnO

Temperature (*K*)	Langmuir			Separation factor	Freundlich		
	b (L/mg)	*q$_m$* (mg P/g)	R^2	R_L	*N*	*K$_f$* (mg P/g)	R^2
288	0.0863	131.78	0.963	$0.104 < R_L < 0.698$	3.37	18.49	0.968
298	0.0803	168.37	0.967	$0.111 < R_L < 0.714$	2.15	23.84	0.981
308	0.2591	145.33	0.861	$0.037 < R_L < 0.436$	2.15	47.37	0.970

Simultaneously, the *n* values obtained from the Freundlich model ranged from 1 to 10, which also implies favorable adsorption of phosphate onto ZnO. In addition, at 308 K, the correlation coefficient R^2 (0.970) suggests that high temperature strengthened the adsorption process, which led to disordered, overlapped distributions of phosphate ions on the surface of the ZnO particles, or chemical reaction between ZnO and phosphate to form crystals of zinc phosphate.

The *q$_m$* values might not provide an accurate estimation of the long-term sorption capacity, but could still be useful for comparing alternative materials. As shown in Table 3, the adsorption capacity was 168.4 mg P/g for ZnO, which is much higher than most of the other adsorbents reported before, and suggests that ZnO has a relatively high potential for use as a phosphate adsorbent.

Thermodynamics

The thermodynamic parameters ($\Delta G°$, $\Delta H°$ and $\Delta S°$) were calculated according to the following equations (Equations (8) and (9)) (Deng & Yu 2012) to evaluate the thermodynamic feasibility and the nature of the adsorption process.

$$\Delta G° = -RT \ln K_d \tag{8}$$

$$\ln K_d = \frac{\Delta S°}{R} - \frac{\Delta H°}{RT} \tag{9}$$

where $\Delta G°$, $\Delta H°$ and $\Delta S°$ are the free energy of sorption (kJ/mol), the standard enthalpy change (kJ/mol) and entropy change (J/(mol·K), respectively, *T* (K) is the absolute temperature in Kelvin, *R* (8.314 J/(mol·K)) is the universal gas constant, K_d is the thermodynamic equilibrium constant, and $\Delta H°$ and $\Delta S°$ were determined as the slope and intercept of the linear plot of lnK_d vs. *1/T*, respectively.

As shown in Figure 5 and Table 4, the values of $\Delta G°$, which indicate the spontaneity degree of the sorption process, are negative (−3.15 to −1.87 kJ/mol) and decreased gradually with the increasing temperature, suggesting that the adsorption process was spontaneous and was enhanced

Table 3 │ Maximum phosphate adsorption capacity of different metal oxide adsorbents

Adsorbent	Adsorption capacity (mg P/g)	*T* (*K*)	pH	Reference
ZnO	168.4	298	6.2	Present study
Fe-Al-Mn trimetal oxides	48.3	298	6.8	Lv *et al.* (2013)
Zn-Al oxides (573 K)	40.8	–	6.8	Cheng *et al.* (2009)
Zn-Al LDH (C$_{urea}$ = 0.4 M)	76.1	303	7	Zhou *et al.* (2011)
Zn-Al LDO (573 K, C$_{urea}$ = 0.4 M)	232.0	303	7	Zhou *et al.* (2011)
ZnCl$_2$-activated coir pith carbon	5.1	308	–	Namasivayam & Sangeetha (2004)
Manganese ore tailings	26.3	298	6	Liu *et al.* (2012)
Pseudo-boehmite (γ-Al$_2$O$_3$)	13.6	293	4.0	Yang *et al.* (2007)
Al-Fe oxide (343 K)	71.6	–	4.8	Harvey & Rhue (2008)
Fe(III)–Cu(II) binary oxides	35.2	298	7.0	Li *et al.* (2014)

– Not explicitly mentioned in the reference.
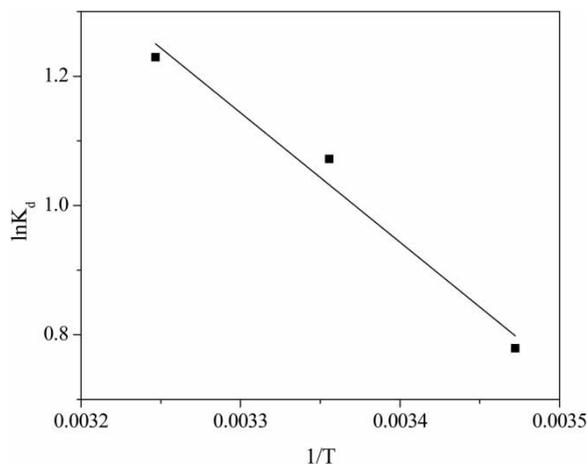
**Figure 5** │ Van't Hoff plot for phosphate adsorption onto ZnO.

Table 4 │ Thermodynamic parameters for phosphate adsorption on ZnO

Temperature (K)	K_d	$\Delta G°$ (kJ/mol)	$\Delta H°$ (kJ/mol)	$\Delta S°$ (J/mol·K)
288	2.18	−1.87	16.65	64.46
298	2.92	−2.51		
308	3.42	−3.15		

with the increasing temperature. The capacity for ZnO particles to adsorb phosphate also increased with increasing temperature (see Figure 4), which also supports this conclusion. The positive value of $\Delta H°$ (16.65 kJ/mol) demonstrates the endothermic nature of the reaction. The positive $\Delta S°$ value obtained (64.46 J/(mol·K)) indicates the degree of disorder, and the increase of randomness due to the increase in the number of species at the solid/liquid interface when the phosphate moves from the hydrous phase to the surface of the adsorbent (Wang *et al.* 2006).

Effect of solution pH and sorption mechanism

The effect of pH on phosphate removal by ZnO was investigated at pH values ranging from 3 to 11. It is clear from Figure 6 that the adsorption is strongly dependent on pH value, and the adsorption capacity decreased significantly with the increasing pH value. The maximum adsorption capacity was about 50 mg P/g at pH ∼ 3.1, which was over 15 times that at pH ∼ 10.6. However increased pH value was found in the final solution after 690 min adsorption at
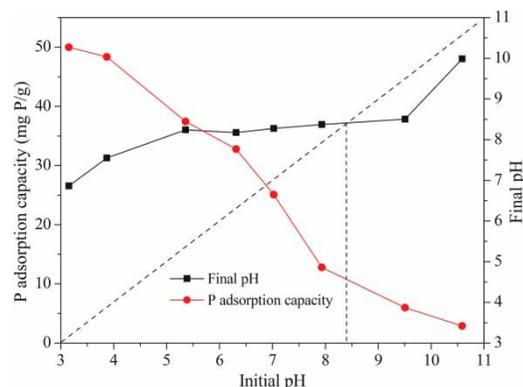
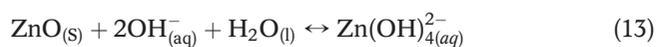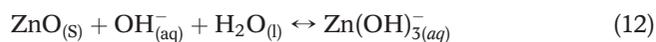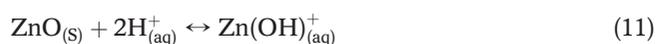**Figure 6** │ Effect of solution pH on phosphate adsorption onto ZnO.

an initial pH from 3 to 8.4 but this decreased at initial pH from 8.4 to 11.

Phosphate exists in aqueous solution as different species, i.e., $H_3PO_4/H_2PO_4^-/HPO_4^{2-}/PO_4^{3-}$. The surface group properties of ZnO are associated with the point of zero charge (pH_{pzc}), and variations of speciation distributions are attributed to the changes of solution pH. pH_{pzc} values were determined by the pH-drift method described by Yang *et al.* (2004) and Liu *et al.* (2011). As can be seen from Figure 6, the pH_{pzc} for ZnO is around 8.4. When solution pH is lower than 8.4, the surface of ZnO could be protonated as $\equiv$Zn-OH + $H^+ \leftrightarrow \equiv$Zn-OH$_2^+$, where $\equiv$Zn-OH represents the uncharged surface group, and $\equiv$Zn-OH$_2^+$ represents the positively charged surface group. The positively charged surface groups are easier to replace at a lower pH from the metal binding sites than hydroxyl groups, which could facilitate the ligand exchange process (Chubar *et al.* 2005; He *et al.* 2010). Moreover, lower pH is favorable for phosphate adsorption through enlarging protonation to boost the positively charged sites, and thus leads to higher phosphate adsorption capacities. Simultaneously, anionic phosphate could interact with the positively charged surface group by electrostatic forces. However, with increasing pH value, HPO_4^{2-} becomes the dominant species instead of $H_2PO_4^-$, progressively, and the capacity for continuous protonation is weakened, which leads to the decline of positively charged sites, and contributes to the decline in the ability of ZnO to adsorb for phosphate.

When solution pH is higher than 8.4, the dominant species are PO_4^{3-} and HPO_4^{2-}, where the deprotonation of $\equiv$Zn-OH, i.e., $\equiv$Zn-OH $-$ $H^+ \leftrightarrow \equiv$Zn-O$^-$ + H^+ exists, where

$\equiv$Zn-O$^-$ represents the negatively charged surface group. The strong electrostatic repulsion between the two negative species Zn-O$^-$ and HPO$_4^-$ become more dominant, which prevents HPO$_4^-$ from adsorbing onto the surface of ZnO. At the same time, the ligand exchange becomes weaker (He *et al.* 2010) because of deprotonation of the adsorbent, and the Lewis acid-base interaction is strengthened due to the increased numbers of oxygen anions in the different ionic forms of phosphate (Zhang *et al.* 2012). With increasing pH, the Lewis acid-base interaction dominates the adsorption process. There existed strong electrostatic repulsion between the surface of the adsorbent and the more negative-charged HPO$_4^{2-}$. At the same time, there was competition between the negatively charged phosphate species and the hydroxide groups adsorbed onto the more negatively charged adsorbent (Huang *et al.* 2013), and phosphate adsorption by electrical force might not occur. All these reasons led to the capacity for phosphate adsorption to drop to the minimum point, i.e., 2.9 mg P/g.

As an environment-friendly engineered material, it is difficult to ignore the solubility of ZnO in acid or base solutions, which is shown in Figure S4 (available online at http://www.iwaponline.com/jwh/013/210.pdf). For a better understanding of the following analysis, the equations below are suggested (Miao *et al.* 2010; Bian *et al.* 2011):

$$ZnO_{(s)} + 2H^+_{(aq)} \leftrightarrow Zn^{2+}_{(aq)} + H_2O_{(l)} \tag{10}$$

$$ZnO_{(S)} + 2H^+_{(aq)} \leftrightarrow Zn(OH)^+_{(aq)} \tag{11}$$

$$ZnO_{(S)} + OH^-_{(aq)} + H_2O_{(l)} \leftrightarrow Zn(OH)^-_{3(aq)} \tag{12}$$

$$ZnO_{(S)} + 2OH^-_{(aq)} + H_2O_{(l)} \leftrightarrow Zn(OH)^{2-}_{4(aq)} \tag{13}$$

Phosphate with a low P/Zn molar ratio would reduce the release of Zn^{2+} into aqueous solution rapidly and substantially (Lv *et al.* 2012), and in this work, the fact that the concentration of the released Zn^{2+} was low might be due to a high P/Zn molar ratio in the working solution. The existence of Zn^{2+} or Zn(OH)$^+$ in the acidic solution could enhance the removal efficiency through the precipitation of zinc phosphate or a combination of Zn(OH)$^+$ and HPO$_4^{2-}$/H$_2$PO$_4^-$ in the acid solution. Otherwise, the appearance of Zn(OH)$_3^-$ or Zn(OH)$_4^{2-}$

could restrain the removal efficiency by electrostatic repulsion. In addition, the attachment of Zn(OH)$_3^-$ or Zn(OH)$_4^{2-}$ onto the surface of ZnO also leads to a decrease in removal efficiency.

Effect of co-existing anions

Competitive sorption is an important factor that influences the removal efficiency. Anions such as CO$_3^{2-}$, SO$_4^{2-}$, NO$_3^-$ and Cl$^-$ commonly exist in water and wastewater, and might interfere with the adsorption of phosphate by competing for sorptive sites on the surface of adsorbents. As shown in Figure 7, SO$_4^{2-}$, NO$_3^-$ and Cl$^-$ do not show any negative effects on phosphate adsorption at concentrations from 0 to 20 mg/L. Anions such as SO$_4^{2-}$ are often weakly bounded with surface sites of metal hydroxides to form outer-sphere surface complexes, but phosphates are relatively strongly bounded with the surface sites forming inner-sphere surface complexes (Zhang *et al.* 2008), so the phosphate adsorption process is barely affected by SO$_4^{2-}$, NO$_3^-$ and Cl$^-$. However, Rahnemaie *et al.* (2007) suggested that carbonate was able to act as a competitor for phosphate at a relatively high concentration. The removal efficiency decreased from 96.5% to 53.5% when the concentration of CO$_3^{2-}$ was increased from 0 to 20 mg/L, which was probably due to the higher affinity of CO$_3^{2-}$ to the surface of ZnO to form CO$_3^{2-}$ CO$_3^{2-}$ or $\equiv$ Zn-OH$_2^+$ HCO$_3^-$. According to the solubility product constants of zinc carbonate ($K_{sp} = 1.46 \times 10^{-10}$) and zinc phosphate ($K_{sp} = 9.1 \times 10^{-33}$) (Lide 1997-1998), zinc phosphate was easier to precipitate and more settlable in water solution. However, the addition of
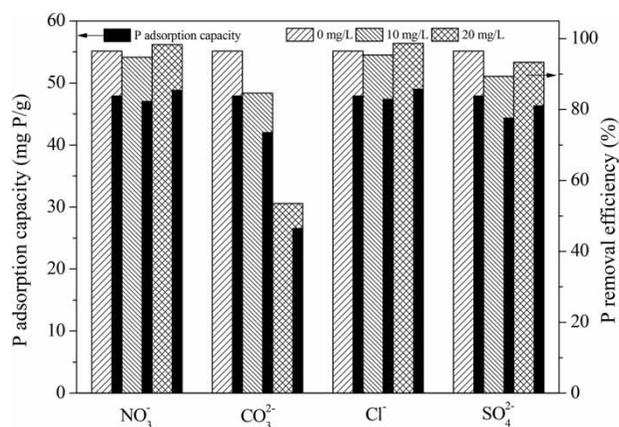

Figure 7 | Effect of co-existing anions on phosphate adsorption onto ZnO.

carbonate decreased the phosphate removal efficiency, suggesting that phosphate adsorption onto ZnO might not be caused by chemical precipitation but rather by chemical adsorption through exchange with OH^- on the hydroxylation surface of ZnO. However, carbonate addition during the adsorption process that consumed some H^+ and improved solution pH values also decreased the phosphate removal efficiency.

CONCLUSIONS

In the present study, ZNO was synthesized using the chemical precipitation-thermal decomposition method to investigate its capacity for phosphate adsorption. The obtained ZnO particles were well crystallized and exhibited individual, sheet morphologies. ZnO has a strong phosphorus removal ability of 163.4 mg/g and the dominant phosphate removal mechanism was probably due to adsorption rather than precipitation. Adsorption of phosphate was highly pH-dependent, and the adsorption capacity decreased with increasing pH. At the same time, Lewis acid-base interaction took the place of ligand exchange to be the dominant mechanism. CO_3^{2-} significantly affected phosphate adsorption due to the higher affinity of CO_3^{2-} for the surface of ZnO. Adsorption performance analysis can provide valuable information, representing practical value for the technological applications of phosphorus removal from aqueous solutions.

ACKNOWLEDGEMENTS

REFERENCES

Arai, Y. & Sparks, D. L. 2001 ATR–FTIR spectroscopic investigation on phosphate adsorption mechanisms at the ferrihydrite-water interface. *J. Colloid Interf. Sci.* **241**, 317–326.

Bian, S. W., Mudunkotuwa, I. A., Rupasinghe, T. & Grassian, V. H. 2011 Aggregation and dissolution of 4 nm ZnO nanoparticles in aqueous environments: influence of pH, ionic strength, size, and adsorption of humic acid. *Langmuir* **27**, 6059–6068.

Cheng, X., Huang, X., Wang, X., Zhao, B., Chen, A. & Sun, D. 2009 Phosphate adsorption from sewage sludge filtrate using zinc-aluminum layered double hydroxides. *J. Hazard. Mater.* **169**, 958–964.

Chouyyok, W., Wiacek, R. J., Pattamakomsan, K., Sangvanich, T., Grudzien, R. M., Fryxell, G. E. & Yantasee, W. 2010 Phosphate removal by anion binding on functionalized nanoporous sorbents. *Environ. Sci. Technol.* **44**, 3073–3078.

Chubar, N. I., Kanibolotskyy, V. A., Strelko, V. V., Gallios, G. G., Samanidou, V. F., Shaposhnikova, T. O., Milgrandt, V. G. & Zhuravlev, I. Z. 2005 Adsorption of phosphate ions on novel inorganic ion exchangers. *Colloid Surface A* **255**, 55–63.

Del Bubba, M., Arias, C. & Brix, H. 2003 Phosphorus adsorption maximum of sands for use as media in subsurface flow constructed reed beds as measured by the Langmuir isotherm. *Water Res.* **37**, 3390–3400.

Deng, H. & Yu, X. 2012 Adsorption of fluoride, arsenate and phosphate in aqueous solution by cerium impregnated fibrous protein. *Chem. Eng. J.* **184**, 205–212.

Foo, K. & Hameed, B. 2010 Insights into the modeling of adsorption isotherm systems. *Chem. Eng. J.* **156**, 2–10.

Haghseresht, F., Wang, S. & Do, D. 2009 A novel lanthanum-modified bentonite, Phoslock, for phosphate removal from wastewaters. *Appl. Clay Sci.* **46**, 369–375.

Hariharan, C. 2006 Photocatalytic degradation of organic contaminants in water by ZnO nanoparticles. *Applied Catalysis A: General* **304**, 55–61.

Harvey, O. R. & Rhue, R. D. 2008 Kinetics and energetics of phosphate sorption in a multi-component Al(III)-Fe(III) hydr (oxide) sorbent system. *J. Colloid Interf. Sci.* **322**, 384–393.

He, H. M., Kang, H. L., Ma, S. L., Bai, Y. X. & Yang, X. J. 2010 High adsorption selectivity of ZnAl layered double hydroxides and the calcined materials toward phosphate. *J. Colloid Interf. Sci.* **343**, 225–231.

Huang, W. Y., Zhu, R. H., He, F., Li, D., Zhu, Y. & Zhang, Y. M. 2013 Enhanced phosphate removal from aqueous solution by ferric-modified laterites: equilibrium, kinetics and thermodynamic studies. *Chem. Eng. J.* **228**, 679–687.

Jiang, J. Q. & Ashekuzzaman, S. 2012 Development of novel inorganic adsorbent for water treatment. *Curr. Opin. Chem. Eng.* **1**, 191–199.

Kikuchi, Y., Qian, Q., Machida, M. & Tatsumoto, H. 2006 Effect of ZnO loading to activated carbon on Pb(II) adsorption from aqueous solution. *Carbon* **44**(2), 195–202.

Li, G., Gao, S., Zhang, G. & Zhang, X. 2014 Enhanced adsorption of phosphate from aqueous solution by nanostructured iron(III)–copper(II) binary oxides. *Chem. Eng. J.* **235**, 124–131.

Liao, X. P., Ding, Y., Wang, B. & Shi, B. 2006 Adsorption behavior of phosphate on metal-ions-loaded collagen fiber. *Ind. Eng. Chem. Res.* **45**, 3896–3901.

Lide, D. R. 1997–1998 *Handbook of Chemistry and Physics*, 78th edn. CRC press, Florida, USA.

Liu, J., Wan, L., Zhang, L. & Zhou, Q. 2011 Effect of pH, ionic strength, and temperature on the phosphate adsorption onto lanthanum-doped activated carbon fiber. *J. Colloid Interf. Sci.* **364**, 490–496.

Liu, T., Wu, K. & Zeng, L. 2012 Removal of phosphorus by a composite metal oxide adsorbent derived from manganese ore tailings. *J. Hazard. Mater.* **217–218**, 29–35.

Liufu, S., Xiao, H. & Li, Y. 2004 Investigation of PEG adsorption on the surface of zinc oxide nanoparticles. *Powder Technol.* **145**, 20–24.

Lv, J. T., Zhang, S. Z., Luo, L., Han, W., Zhang, J., Yang, K. & Christie, P. 2012 Dissolution and microstructural transformation of ZnO nanoparticles under the influence of phosphate. *Environ. Sci. Technol.* **46**, 7215–7221.

Lv, J. B., Liu, H., Liu, R., Zhao, X. L. & Qu, J. H. 2013 Adsorptive removal of phosphate by a nanostructured Fe–Al–Mn trimetal oxide adsorbent. *Powder Technol.* **233**, 146–154.

Miao, A. J., Zhang, X. Y., Luo, Z. P., Chen, C. S., Chin, W. C., Santschi, P. H. & Quigg, A. 2010 Zinc oxide-engineered nanoparticles: dissolution and toxicity to marine phytoplankton. *Environ. Toxicol. Chem.* **29**, 2814–2822.

Moezzi, A., McDonagh, A. M. & Cortie, M. B. 2012 Zinc oxide particles: synthesis, properties and applications. *Chem. Eng. J.* **185**, 1–22.

Mohan, D. & Pittman Jr, C. U. 2007 Arsenic removal from water/wastewater using adsorbents-A critical review. *J. Hazard. Mater.* **142**, 1–53.

Morse, G., Brett, S., Guy, J. & Lester, J. 1998 Review: phosphorus removal and recovery technologies. *Sci. Total. Environ.* **212**, 69–81.

Musić, S., Popović, S., Maljković, M. & Dragčević, Đ. 2002 Influence of synthesis procedure on the formation and properties of zinc oxide. *Mater. Chem. Phy.* **77**, 521–530.

Namasivayam, C. & Sangeetha, D. 2004 Equilibrium and kinetic studies of adsorption of phosphate onto $ZnCl_2$ activated coir pith carbon. *J. Colloid Int. Sci.* **280**, 359–365.

Ning, Z. L., Li, W. J., Sun, C. Y., Che, P. & Chang, Z. D. 2013 Synthesis and optical properties of zinc phosphate microspheres. *Trans. Nonferrous Met. Soc. China* **23**, 718–724.

Pitakteeratham, N., Hafuka, A., Satoh, H. & Watanabe, Y. 2013 High efficiency removal of phosphate from water by zirconium sulfate surfactant micelle mesostructure immobilized on polymer matrix. *Water Res.* **47**, 3583–3590.

Prasad, V., Souza, C. D., Yadav, D., Shaikh, A. & Vigneshwaran, N. 2006 Spectroscopic characterization of zinc oxide nanorods synthesized by solid-state reaction. *Spectrochim. Acta. A* **65**, 173–178.

Rahnemaie, R., Hiemstra, T. & Riemsdijk, W. H. 2007 Carbonate adsorption on goethite in competition with phosphate. *J. Colloid Interf. Sci.* **315**, 415–425.

Rentz, J. A., Turner, I. P. & Ullman, J. L. 2009 Removal of phosphorus from solution using biogenic iron oxides. *Water Res.* **43**, 2029–2035.

Tsuji, M. 2002 Seo_3^{2-} selective properties of inorganic materials synthesized by the soft chemical process. *Solid State Ionics* **151**, 385–392.

Vohla, C., Kõiv, M., Bavor, H. J., Chazarenc, F. & Mander, Ü. 2011 Filter materials for phosphorus removal from wastewater in treatment wetlands – a review. *Ecol. Eng.* **37**, 70–89.

Wan, Q. 2006 Structural and magnetic properties of manganese and phosphorus codoped ZnO films on (0001) sapphire substrates. *Appl. Phys. Lett.* **89**, 082515–082513.

Wang, X., Yu, J. C., Liu, P., Wang, X., Su, W. & Fu, X. 2006 Probing of photocatalytic surface sites on SO_4^{2-}/TiO_2 solid acids by in situ FT-IR spectroscopy and pyridine adsorption. *J. Photoch. Photobio. A* **179**, 339–347.

Wang, S. L., Cheng, C. Y., Tzou, Y. M., Liaw, R. B., Chang, T. W. & Chen, J. H. 2007 Phosphate removal from water using lithium intercalated gibbsite. *J. Hazard Mater.* **147**, 205–212.

Wang, L., Zheng, Y., Li, X., Dong, W., Tang, W., Chen, B., Li, C., Li, X., Zhang, T. & Xu, W. 2011 Nanostructured porous ZnO film with enhanced photocatalytic activity. *Thin Solid Films* **519** (16), 5673–5678.

Yang, Y., Chun, Y., Sheng, G. & Huang, M. 2004 pH-dependence of pesticide adsorption by wheat-residue-derived black carbon. *Langmuir* **20**, 6736–6741.

Yang, X., Wang, D., Sun, Z. & Tang, H. 2007 Adsorption of phosphate at the aluminum (hydr) oxides-water interface: role of the surface acid–base properties. *Colloid Surface A* **297**, 84–90.

Yeon, K. H., Park, H., Lee, S. H., Park, Y. M., Lee, S. H. & Iwamoto, M. 2008 Zirconium mesostructures immobilized in calcium alginate for phosphate removal. *Korean J. Chem. Eng.* **25**, 1040–1046.

Zhang, N., Lin, L. S. & Gang, D. 2008 Adsorptive selenite removal from water using iron-coated GAC adsorbents. *Water Res.* **42**, 3809–3816.

Zhang, L., Zhou, Q., Liu, J., Chang, N., Wan, L. & Chen, J. 2012 Phosphate adsorption on lanthanum hydroxide-doped activated carbon fiber. *Chem. Eng. J.* **185–186**, 160–167.

Zhang, H., Xu, M., Wang, H. J., Lei, D., Qu, D. & Zhai, Y. J. 2013 Adsorption of copper by aminopropyl functionalized mesoporous delta manganese dioxide from aqueous solution. *Colloid Surface A* **435**, 78–84.

Zhou, J., Yang, S., Yu, J. & Shu, Z. 2011 Novel hollow microspheres of hierarchical zinc-aluminum layered double hydroxides and their enhanced adsorption capacity for phosphate in water. *J. Hazard. Mater.* **192**, 1114–1121.